3-1-2006

Polarizing properties of embedded symmetric trilayer stacks under conditions of frustrated total internal reflection

Rasheed M.A. Azzam
University of New Orleans, razzam@uno.edu

Siva R. Perla

Recommended Citation

Rasheed M. A. Azzam and Siva R. Perla, "Polarizing properties of embedded symmetric trilayer stacks under conditions of frustrated total internal reflection," Appl. Opt. 45, 1650-1656 (2006)

Polarizing properties of embedded symmetric trilayer stacks under conditions of frustrated total internal reflection

Rasheed M. A. Azzam and Siva R. Perla

An all-transparent symmetric trilayer structure, which consists of a high-index center layer coated on both sides by a low-index film and embedded in a high-index prism, can function as an efficient polarizer or polarizing beam splitter under conditions of frustrated total internal reflection over a wide range of incidence angles. For a given set of refractive indices, all possible solutions for the thicknesses of the layers that suppress the reflection of either the *p* or *s* polarization at a specified angle, as well as the reflectance of the system for the orthogonal polarization, are determined. A 633 nm design that uses a MgF_2–ZnS–MgF_2 trilayer embedded in a ZnS prism achieves an extinction ratio (ER) $>$ 40 dB from 50° to 80° in reflection and an ER $>$ 20 dB from 58° to 80° in transmission. IR polarizers that use CaF_2–Ge–CaF_2 trilayers embedded in a ZnS prism are also considered. © 2006 Optical Society of America

OCIS codes: 230.5440, 240.0310, 260.5430, 310.0310.

1. Introduction

Thin-film polarizers and polarizing beam splitters (PBS) are widely known[1–4] and are based on the destructive interference of light for one linear polarization (*p* or *s*) and the nearly full constructive interference for the orthogonal polarization.

In this paper we consider the polarizing properties of a symmetric trilayer stack of refractive indices n_1, n_2, n_1, which is embedded in a high-index medium (prism) of refractive index n_0; see Fig. 1. All media are considered to be transparent, optically isotropic, and separated by parallel-plane boundaries. We also assume that $n_0 > n_1$, $n_2 \geq n_0$ and that light is incident from medium 0 at an angle ϕ_0, which is greater than the critical angle [$\phi_{c01} = \arcsin(n_1/n_0)$] of the 01 interface, so that frustrated total internal reflection (FTIR) takes place.

In a recent paper[5] Li and Dobrowolski reviewed the earlier literature about polarizers that employ FTIR and proposed a new high-performance PBS that reflects the *p* polarization and transmits the *s* polarization. (In the conventional MacNeille design[6,7] that operates at Brewster's angle, the *p* polarization is transmitted and the *s* polarization is reflected.) The Li and Dobrowolski design uses a symmetric trilayer (3) of thin films as a basic unit (period), which is repeated many times (9–27). Therefore the full multilayer consists of as many as 81 thin films.

In Section 2 we consider polarizers that consist of only one period (trilayer), and we do not resort to the thin-film approximation of Ref. 5. Also, instead of using Herpin's equivalent-layer theory,[8,9] we introduce an explicit technique that is based on the full expressions of the complex-amplitude reflection coefficients of the trilayer structure. We also allow for either the *p* or *s* polarization to be reflected or transmitted.

In Section 3 we assume a set of refractive indices, and we determine all possible embedded symmetric trilayers that suppress the reflection of *p*- or *s*-polarized light at each one of several angles of incidence ϕ_0, while boosting the reflection of the orthogonal polarization toward 100%. We find a continuum of solutions at each angle and for each polarization. Results are presented for visible-laser (633 nm) polarizers that use MgF_2–ZnS–MgF_2 trilayers embedded in a Cleartran[10] (ZnS) prism.

In Section 4 a specific trilayer stack is described that functions as a dual polarizer (or PBS) at two widely separated angles of choice (e.g., 55° and 75°).

The authors are with the Department of Electrical Engineering, University of New Orleans, New Orleans, Louisiana 70148. R. M. A. Azzam's e-mail address is razzam@uno.edu.
Received 7 March 2005; accepted 13 August 2005.
0003-6935/06/071650-07$15.00/0

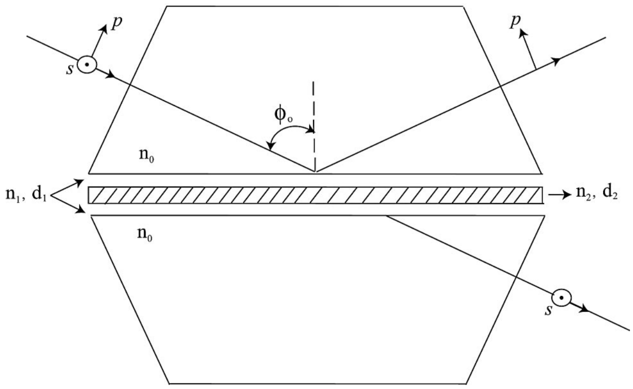

Fig. 1. Embedded trilayer structure as a polarizing beam splitter (PBS). A PBS in which the p polarization is transmitted and the s polarization is reflected is also considered. See text for discussion.

One such MgF_2–ZnS–MgF_2 trilayer embedded in a Cleartran (ZnS) prism achieves an extinction ratio in reflection $ER_r > 40$ dB over the 50°–80° angular range and an extinction ratio in transmission $ER_t > 20$ dB over the 58°–80° range. The angular range measured in air outside the prism is even larger if one accounts for refraction at the entrance face of the prism by using Snell's law. The response of this wide-angle design to a 600–700 nm spectral scan is also considered.

In Section 5 we present results for infrared polarizers that use the CaF_2–Ge–CaF_2 trilayer embedded in a ZnS prism. Finally, Section 6 gives a brief summary of the paper.

2. Design Procedure

Consider a monochromatic light beam traveling in an ambient medium (solid prism) of refractive index n_0 and incident on an embedded symmetric trilayer structure at an angle of incidence ϕ_0 with respect to the normal to the interfaces, as shown in Fig. 1. The overall complex-amplitude reflection coefficient for ν-polarized light ($\nu = p$ or s) can be expressed as[11]

$$r_\nu = \frac{l + mX_1 + nX_2 - mX_1X_2 - nX_1^2 - lX_2X_1^2}{1 + bX_1 + cX_2 + dX_1^2 - bX_1X_2 + eX_2X_1^2}, \quad (1)$$

$$l = r_{01\nu},$$

$$m = r_{12\nu}\,(1 + r_{01\nu}^2),$$

$$n = -r_{01\nu}\, r_{12\nu}^2, \quad (2)$$

$$b = 2r_{01\nu}\, r_{12\nu},$$

$$c = -r_{12\nu}^2,$$

$$d = r_{01\nu}^2 r_{12\nu}^2,$$

$$e = -r_{01\nu}^2. \quad (3)$$

In Eq. (1) X_1 and X_2 are complex exponential functions of film thickness given by

$$X_i = \exp(-j\pi Z_i \cos\phi_i), \quad (4)$$

where Z_i is the thickness of the ith film ($i = 1, 2$) normalized to the quarter-wave thickness at normal incidence, i.e.,

$$Z_i = \frac{4d_i n_i}{\lambda}. \quad (5)$$

In Eq. (4) ϕ_i is the angle of refraction in the ith layer, and in Eq. (5) n_i, d_i are the refractive index and metric thickness of the ith layer, respectively, and λ is the vacuum wavelength of light.

The Fresnel complex-amplitude reflection coefficients of the ij interface for the p and s polarizations are given by[11]

$$r_{ijp} = \frac{n_j \cos\phi_i - n_i \cos\phi_j}{n_j \cos\phi_i + n_i \cos\phi_j}, \qquad r_{ijs} = \frac{n_i \cos\phi_i - n_j \cos\phi_j}{n_i \cos\phi_i + n_j \cos\phi_j}. \quad (6)$$

To suppress the ν polarization on reflection, we set

$$r_\nu = 0 \quad (7)$$

in Eq. (1). This gives us the following constraint between X_1 and X_2:

$$X_2 = \frac{l + mX_1 - nX_1^2}{-n + mX_1 + lX_1^2}. \quad (8)$$

When the refractive indices and angle of incidence are such that $n_1/n_0 < \sin\phi_0$, FTIR takes place at the 01 interface at ϕ_0 and the light field becomes evanescent in medium 1 (the low-index film). In this case $\cos\phi_1$ is pure imaginary, and X_1 is real in the range $0 \le X_1 \le 1$. Because we also choose $n_2 \ge n_0$, the angle of refraction ϕ_2 in the middle layer is real, which makes X_2 a pure phase factor, so that $|X_2| = 1$. For each real value of X_1 in the range $0 \le X_1 \le 1$, we find that $|X_2| = 1$ by using Eq. (8). (An analytical proof of this statement is given in Appendix A.) Therefore there is an infinite number of solutions (X_1, X_2) that satisfy Eq. (8) so that $r_\nu = 0$. The corresponding solution sets of normalized film thicknesses (Z_1, Z_2) are determined subsequently by using Eq. (4).

An acceptable design must have a reflectance

$$R_{\nu'} = |r_{\nu'}|^2 \quad (9)$$

for the orthogonal polarization ν' that is as close as possible to 1. In general this reflectance increases as the normalized thickness Z_1 (of the low-index layers that support the evanescent field) and the angle of incidence ϕ_0 are increased.

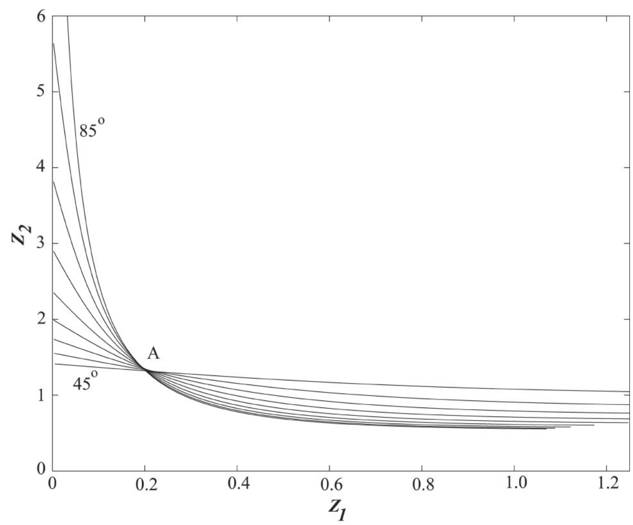

Fig. 2. Plot of Z_2 as a function of Z_1 such that $r_p = 0$ at angles of incidence ϕ_0 from 45° to 85° in steps of 5°. We assume MgF_2–ZnS–MgF_2 trilayers embedded in a ZnS substrate with refractive indices $n_0 = 2.35$ (ZnS), $n_1 = 1.38$ (MgF_2), and $n_2 = 2.35$ (ZnS) in the visible spectrum. Notice that all curves appear to have a common point of intersection at A.

3. MgF_2–ZnS–MgF_2 Trilayer Polarizers for the Visible Spectrum

Figure 2 shows Z_2 as a function of Z_1 such that $r_p = 0$ at angles of incidence ϕ_0 from 45° to 85° in steps of 5° for MgF_2–ZnS–MgF_2 trilayers embedded in a ZnS substrate with refractive indices $n_0 = 2.35$ (ZnS), $n_1 = 1.38$ (MgF_2), and $n_2 = 2.35$ (ZnS) in the visible spectrum.

In Fig. 3 the associated reflectance $R_s = |r_s|^2$ for the s polarization is plotted versus Z_1 at the same angles of incidence as in Fig. 2. It is apparent that R_s increases monontonically with Z_1 at a given ϕ_0 and with ϕ_0 at a given Z_1. Figure 4 shows a magnified view of the region of high reflectance in Fig. 3. Efficient polarizers ($R_s > 99\%$) are readily obtained by using many combinations of Z_1 and ϕ_0.

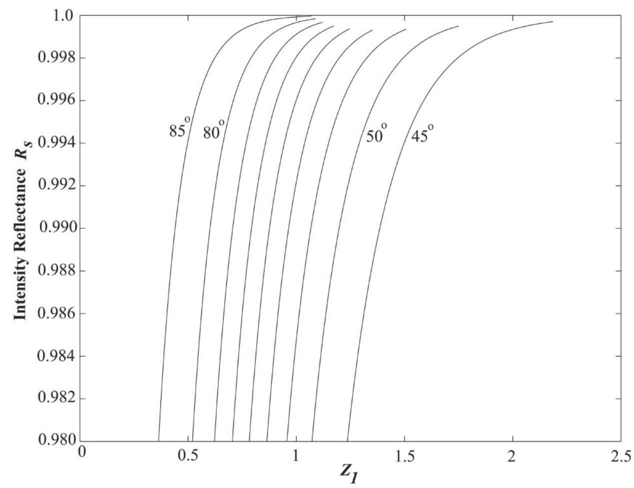

Fig. 4. Magnified view of the region of high reflectance in Fig. 3.

An interesting feature in Fig. 2 is that all the curves appear to pass through one common point A. If this were true, it would signify that one multilayer can force $r_p = 0$ at many angles of incidence simultaneously. However, as Fig. 5 shows, there is not strictly one common point of intersection for all the curves in Fig. 2. Furthermore, because Z_1 at A is small (≈ 0.2), the reflectance R_s of such a wide-angle polarizer is low except at high incidence angles, as is evident from Fig. 3.

We now consider the other class of $r_s = 0$ polarizers by using the same MgF_2–ZnS–MgF_2 trilayer embedded in a ZnS substrate.

Figure 6 shows Z_2 as a function of Z_1 such that $r_s = 0$ at angles of incidence ϕ_0 from 45° to 85° in steps of 5°. In Fig. 7 the corresponding reflectance $R_p = |r_p|^2$ for the p polarization is plotted versus Z_1 at the

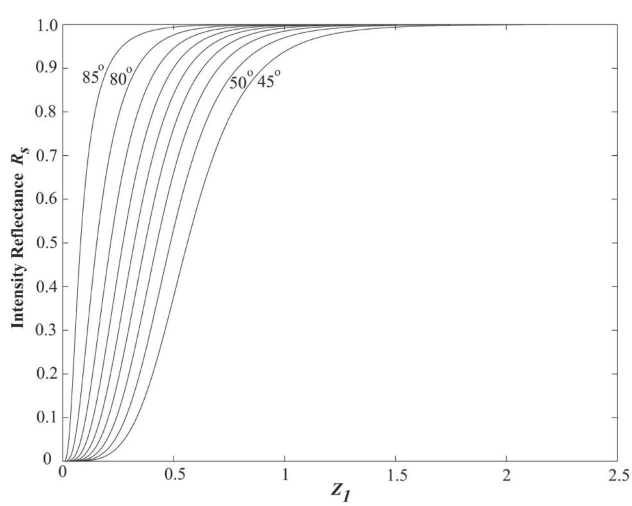

Fig. 3. Reflectance $R_s = |r_s|^2$ for the s polarization is plotted versus Z_1 at the same angles of incidence as in Fig. 2 and under the $r_p = 0$ condition.

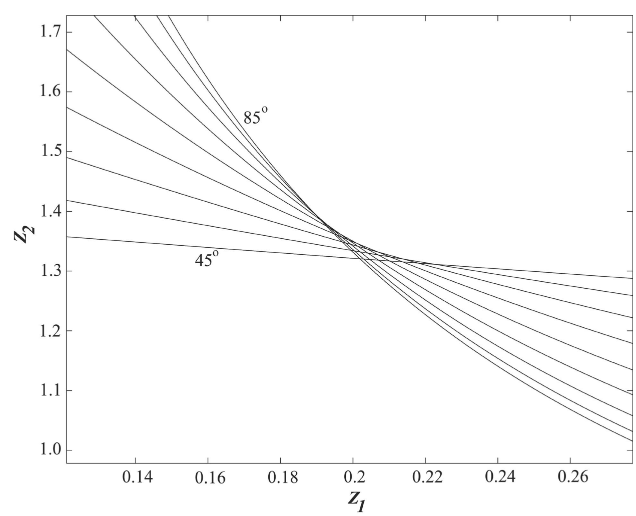

Fig. 5. High-resolution view of the family of curves of Fig. 2 near point A shows that there is not strictly one common point of intersection for all the curves.

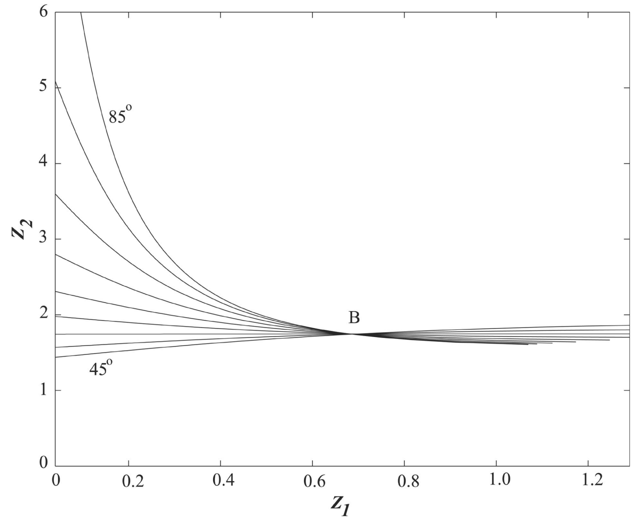

Fig. 6. Plot of Z_2 as a function of Z_1 such that $r_s = 0$ at angles of incidence ϕ_0 from 45° to 85° in steps of 5°. All the curves appear to pass through a common point B.

same angles of incidence. Again we find that R_p increases monontonically with Z_1 at a given ϕ_0 and with ϕ_0 at a given Z_1, as one may intuitively expect.

Efficient polarizers with high ER in transmission ($R_p > 99\%$) are realizable by using many combinations of Z_1 and ϕ_0, as is shown more clearly in Fig. 8.

In Fig. 6 all the curves appear to pass through a common point B. Although this is not strictly true, as is shown in Fig. 9, it still suggests that one and the same multilayer can satisfy the condition $r_s = 0$ accurately (although not exactly) at many angles of incidence simultaneously. The value of Z_1 at B is large enough (≈ 0.7) to make the reflectance $R_p > 90\%$ at all angles $\geq 50°$, as one can see from Fig. 7. This important wide-angle polarizer is considered further in Section 4.

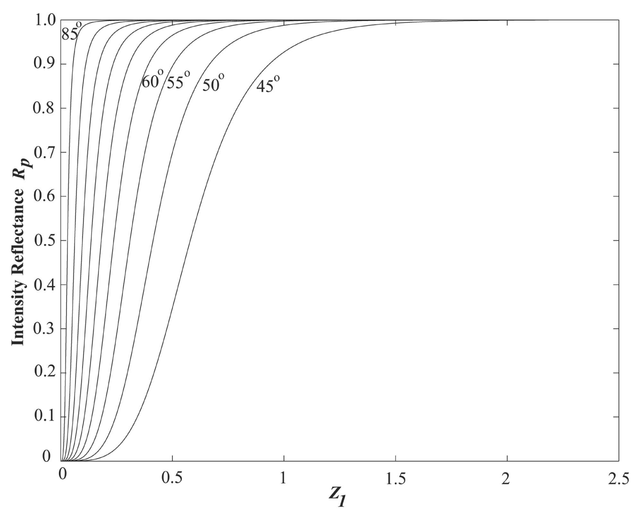

Fig. 7. Reflectance $R_p = |r_p|^2$ for the p polarization is plotted versus Z_1 at the same angles of incidence as in Fig. 6 and under the $r_s = 0$ condition.

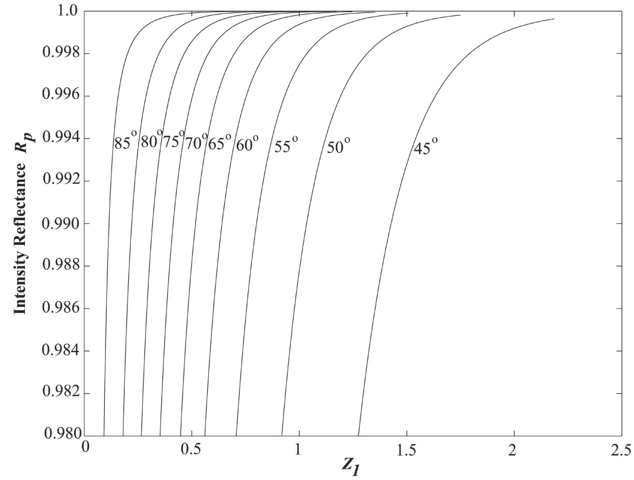

Fig. 8. Expanded view of Fig. 7 in the region of high reflectance.

4. Wide-Angle Polarizer Design

This specific design is based on operation at the point of intersection ($Z_1 = 0.6831$, $Z_2 = 1.7472$) of the two curves in Fig. 6 that correspond to $\phi_0 = 55°$ and 75°. The corresponding metric thicknesses of the MgF_2 and ZnS films, calculated at a wavelength $\lambda = 633$ nm, are $d_1 = 78.305$ nm and $d_2 = 117.618$ nm, respectively.

Figure 10 shows the reflectances R_p and R_s as functions of the angle of incidence ϕ_0 from 40° to 85° when the metric film thicknesses and wavelength are kept constant. Note that $R_s < 0.002$ over this entire range of angles and that $R_p > 90\%$ for $\phi_0 > 52°$.

In Fig. 11 the extinction ratios in reflection and transmission (ER_r and ER_t in decibels) are plotted versus the angle of incidence ϕ_0 from 50° to 80°. Good polarization properties ($ER_r > 40$ dB and $ER_t > 20$ dB) are achieved over an extended range of angles. If one accounts for the refraction of light from air to the

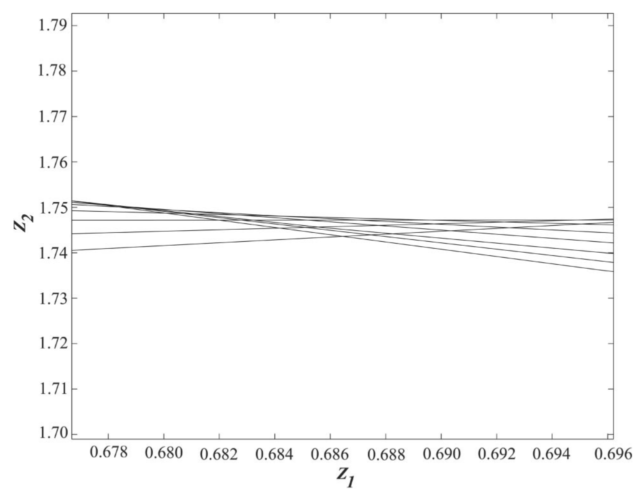

Fig. 9. Magnified view of the family of curves of Fig. 6 in the neighborhood of point B shows that there is not strictly one common point of intersection for all the curves.

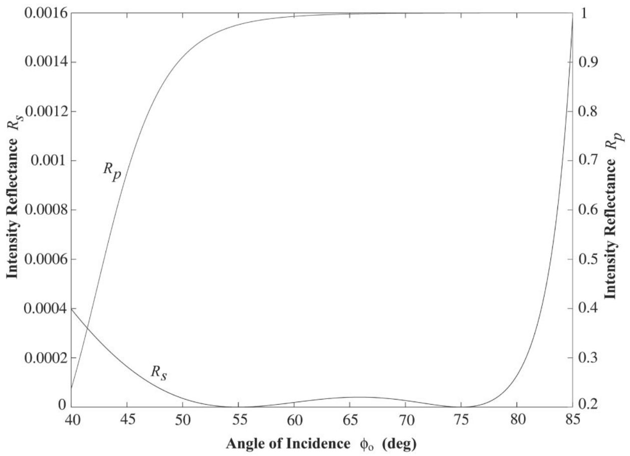

Fig. 10. Reflectances R_p and R_s as functions of the angle of incidence ϕ_0 from 40° to 85° for a polarizer using a MgF_2–ZnS–MgF_2 trilayer embedded in a ZnS substrate with refractive indices $n_0 = 2.35$ (ZnS), $n_1 = 1.38$ (MgF_2), and $n_2 = 2.35$ (ZnS). The metric film thicknesses ($d_1 = 78.31$ nm, $d_2 = 117.62$ nm) and wavelength (633 nm) are kept constant.

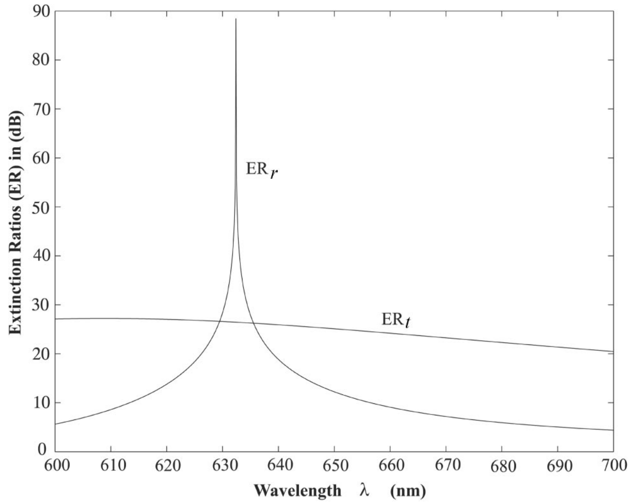

Fig. 12. Extinction ratios ER_r and ER_t in decibels as functions of wavelength λ for the wide-angle polarizer of Fig. 10. The metric film thicknesses ($d_1 = 78.31$ nm, $d_2 = 117.62$ nm) and angle of incidence ϕ_0 (65°) are kept constant.

high-index ZnS substrate, the angular bandwidth in air is even larger that that indicated by Fig. 11.

Although this wide-angle polarizer is intended for use with monochromatic (633 nm) light, it is of interest to consider its performance over a range of wavelengths. For this purpose, the metric film thicknesses $d_1 = 78.305$ nm and $d_2 = 117.618$ nm and the angle of incidence $\phi_0 = 65°$ are kept constant, and the wavelength λ is scanned over the 600–700 nm range. In this calculation the dispersion of MgF_2 and ZnS over this limited spectral range is ignored. Figure 12 shows the extinction ratios ER_r and ER_t in decibels as functions of λ. Note that ER_t remains greater than 20 dB over this 100 nm bandwidth, whereas ER_r is high only in the immediate neighborhood of the design wavelength (633 nm).

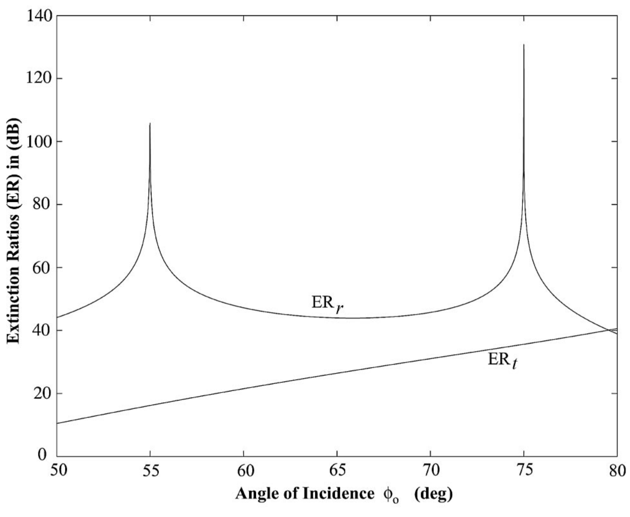

Fig. 11. Extinction ratios in reflection and transmission (ER_r and ER_t) in decibels are plotted versus the angle of incidence ϕ_0 from 50° to 80° for the wide-angle polarizer of Fig. 10.

5. CaF_2–Ge–CaF_2 Trilayer Infrared Polarizers

Figure 13 shows the constraint between Z_2 and Z_1 such that $r_p = 0$ at angles of incidence ϕ_0 from 45° to 85° in 5° steps for CaF_2–Ge–CaF_2 trilayers embedded in a ZnS substrate with refractive indices $n_0 = 2.2$ (ZnS), $n_1 = 1.4$ (CaF_2), and $n_2 = 4$ (Ge) in the infrared. The family of curves in Fig. 13 is substantially different from that of Fig. 2 for the MgF_2–ZnS–MgF_2 trilayer polarizers in the visible spectrum under the same $r_p = 0$ condition, and a common (or near-common) point of intersection among all the curves does not exist. This significant change is due mostly to the substantially higher refractive index of the center layer (Ge, $n_2 = 4$).

Figure 14 shows the associated reflectance R_s =

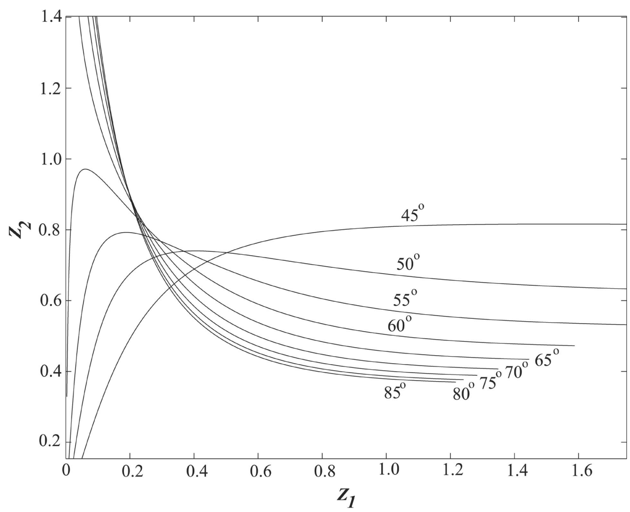

Fig. 13. Constraint between Z_2 and Z_1 such that $r_p = 0$ at angles of incidence ϕ_0 from 45° to 85° in 5° steps for CaF_2–Ge–CaF_2 trilayers embedded in a ZnS substrate with refractive indices $n_0 = 2.2$ (ZnS), $n_1 = 1.4$ (CaF_2), and $n_2 = 4$ (Ge) in the infrared.

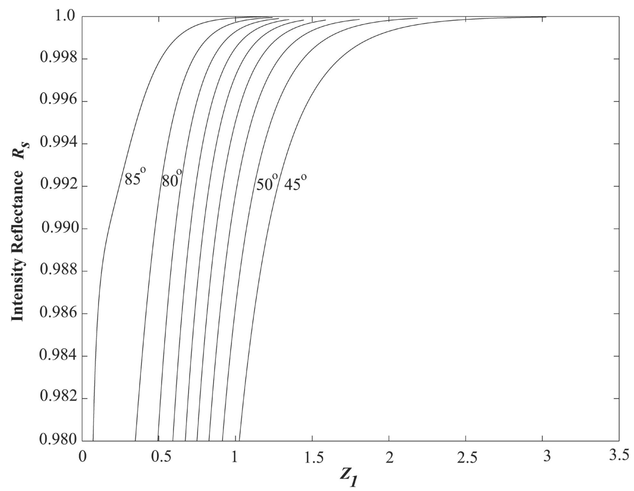

Fig. 14. Reflectance $R_s = |r_s|^2$ for the s polarization plotted versus Z_1 under the $r_p = 0$ condition and at the same angles of incidence as in Fig. 13.

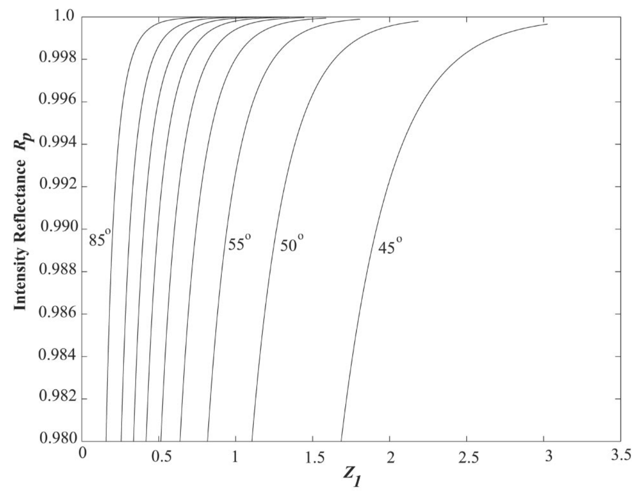

Fig. 16. Reflectance $R_p = |r_p|^2$ for the p polarization plotted versus Z_1 under the $r_s = 0$ condition and at the same angles of incidence as in Fig. 15.

$|r_s|^2$ for the s polarization plotted versus Z_1 at the same angles of incidence as in Fig. 13. Again, R_s increases monontonically with Z_1 at a given ϕ_0 and with ϕ_0 at a given Z_1. Efficient polarizers ($R_s > 99\%$) are readily obtained for many combinations of Z_1 and ϕ_0.

Figure 15 shows Z_2 versus Z_1 such that $r_s = 0$ at angles of incidence ϕ_0 from 45° to 85° in 5° steps for the same CaF_2–Ge–CaF_2 trilayers embedded in ZnS substrate in the infrared. All the curves in Fig. 15 appear to share a common point of intersection C. The associated reflectance $R_p = |r_p|^2$ for the p polarization is plotted versus Z_1 at the same angles as in Fig. 16. A wide-angle infrared polarizer that is based on operation at point C of Fig. 15 is possible, and its performance is comparable with that of the visible polarizer discussed in Section 4.

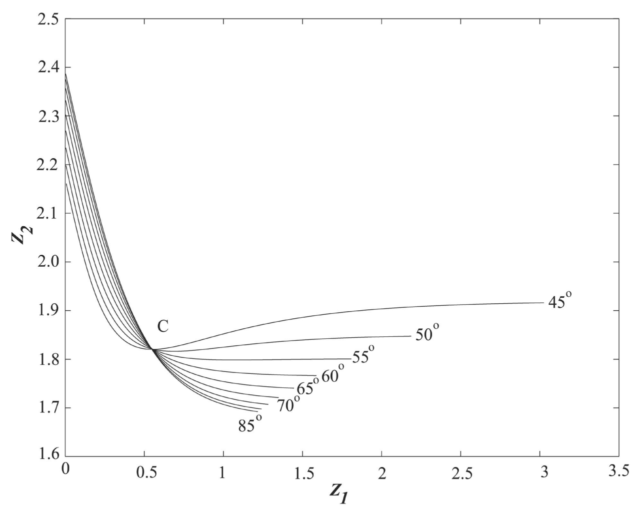

Fig. 15. Plot of Z_2 versus Z_1 such that $r_s = 0$ at angles of incidence ϕ_0 from 45° to 85° in 5° steps for CaF_2–Ge–CaF_2 trilayers embedded in ZnS substrate in the infrared. All the curves appear to share a common point of intersection at C.

6. Summary

The polarizing properties of a symmetric trilayer stack embedded in a high-index prism are thoroughly examined by using analytical and numerical calculations. All possible solutions (infinite in number) that suppress the p or s polarization in reflection are determined, and the associated throughput for the orthogonal polarization is calculated. Conditions for obtaining wide-angle designs are clearly demonstrated.

Presented are specific examples of polarizers for the visible spectrum that use MgF_2–ZnS–MgF_2 trilayers embedded in a ZnS prism to achieve extinction ratios greater than 40 dB in reflection and greater than 20 dB in transmission over a wide range of incidence angles. Infrared polarizers that use CaF_2–Ge–CaF_2 trilayers embedded in a ZnS prism are also considered.

Appendix A

In this Appendix we prove that, for each real value of X_1 in the range $0 \le X_1 \le 1$, X_2 as given by Eq. (8) is a pure phase factor; hence $|X_2| = 1$. To do this we substitute l, m, and n from Eqs. (2) into Eq. (8) and cast the result in the following form:

$$X_2 = (r_{12}{}^2)\, \frac{r_{12}{}^{-2} + r_{12}{}^{-1}(r_{01}{}^{-1} + r_{01})X_1 + X_1{}^2}{r_{12}{}^2 + r_{12}(r_{01}{}^{-1} + r_{01})X_1 + X_1{}^2}. \quad \text{(A1)}$$

Under conditions of FTIR, all interface reflection coefficients are pure phase factors; hence

$$r_{ij} = \exp(j\delta_{ij}),$$

$$r_{ij}{}^{-1} = r_{ij}{}^* = \exp(-j\delta_{ij}),$$

$$r_{ij}{}^{-1} + r_{ij} = 2\cos(\delta_{ij}), \quad \text{(A2)}$$

where δ_{ij} is the interface reflection phase shift.[12] Equations (A2), and the fact that X_1 is real, allow Eq. (A1) to be written as

$$X_2 = (r_{12}{}^2)(W/W^*). \tag{A3}$$

Because each of the bracketed terms in Eq. (A3) is a pure phase factor, it follows that

$$|X_2| = 1. \tag{A4}$$

For simplicity the polarization subscript ν was dropped in Eqs. (A1)–(A3).

We thank Amrit De for his participation in the initial phase of this project.

References

1. H. A. Macleod, *Thin Film Optical Filters,* 2nd ed. (McGraw-Hill, 1986).
2. A. Thelen, *Design of Optical Interference Coatings* (McGraw-Hill, 1988).
3. J. A. Dobrowolski, "Optical properties of films and coatings," in *Handbook of Optics,* Vol. I, M. Bass, E. W. van Stryland, D. R. Williams, and W. L. Wolfe, eds. (McGraw-Hill, 1995).
4. J. M. Bennett, "Polarizers," in *Handbook of Optics,* Vol. II, M. Bass, E. W. van Stryland, D. R. Williams, and W. L. Wolfe, eds. (McGraw-Hill, 1995).
5. L. Li and J. A. Dobrowolski, "High-performance thin-film polarizing beam splitter operating at angles greater than the critical angle," Appl. Opt. **39,** 2754–2771 (2000).
6. S. M. MacNeille, "Beam splitter," U.S. patent 2,403,731 (6 July 1946).
7. M. Banning, "Practical methods of making and using multilayer filters," J. Opt. Soc. Am. **37,** 792–797 (1947).
8. L. I. Epstein, "The design of optical filters," J. Opt. Soc. Am. **42,** 806–810 (1952).
9. M. C. Ohmer, "Design of three-layer equivalent films," J. Opt. Soc. Am. **68,** 137–139 (1978).
10. CVD, Inc., 35 Industrial Parkway, Woburn, Mass. 01801.
11. R. M. A. Azzam and N. M. Bashara, *Ellipsometry and Polarized Light* (North-Holland, 1987).
12. R. M. A. Azzam, "Phase shifts that accompany total internal reflection at a dielectric–dielectric interface," J. Opt. Soc. Am. A **21,** 1559–1563 (2004).